Geotech Geol Eng (2022) 40:5397–5409
https://doi.org/10.1007/s10706-022-02221-7

ORIGINAL PAPER

Couple Effect of Joint Pore Pressure and Joint Orientations on Rock Strength Based on Numerical Modeling

Gaobo Zhao · Wenbing Guo · Lingyun Kong · Yun Zhao · Qingwen Shi

Received: 27 April 2022 / Accepted: 15 June 2022 / Published online: 2 July 2022

Abstract The joint pore pressure inside rock mass significantly affects groundwater bursting. To investigate the couple effect of joint pore pressure and joint orientations on rock strength, this study utilized the three-dimensional numerical modeling code of 3DEC to carry out the experiments of uniaxial and triaxial compression tests. Seven three-dimensional models with parallel oriented joints of 0°, 15°, 30°, 45°, 60°, 75°, 90° inclination angle were developed. The input parameters of rock, joints and fluid properties were calibrated based on the results of previous studies. The established models were tested in the uniaxial and triaxial compression tests under uncoupled mechanical state and coupled hydro-mechanical state with various joint pore pressures (0.5, 1.0, 2.0, 3.0 MPa). The results show that the strength varied with different joint orientations producing the classic "U"-shaped curve. However, when the joint pore pressure was involved, the strength changed to a "W"-shaped curve. Additionally, the effect of the joint pore pressure on rock strength depends on orientations. The strength was decreasing with the increase of joint pore pressure when the orientations are 0°, 15°, 30°, 75° and 90°; the strength was increasing with the increase of joint pore pressure when the orientation is 60°; the strength was increasing first and then decreasing when the orientation is 45°. The results indicate that the joint orientation plays more important role than joint pore pressure on the strength change, thus needs to be considered for studying groundwater bursting.

Keywords Parallel oriented joints · Joint pore pressure · Rock strength · Numerical modeling

G. Zhao (✉) · Y. Zhao · Q. Shi
Department of Mining Engineering, West Virginia University, Morgantown, WV, USA
e-mail: gz00001@mix.wvu.edu

W. Guo
School of Energy Science and Engineering, Henan Polytechnic University, Jiaozuo 454003, Henan, China

L. Kong
Department of Petroleum Engineering, School of Earth Resources, China University of Geosciences, Wuhan, China

1 Introduction

After longwall mining the overburden strata is disturbed to different degrees, and might form four zones including the caved zone, fractured zone, continuous deformation zone and soil zone (Guo et al. 2019, 2021; Peng et al. 2019; Zhao et al. 2020; Esterhuizen et al. 2021). If aquifers are located in the fractured zone, groundwater bursting, a severe geological hazardous event, will happen because of the pore pressure inside rock mass containing joints, bedding planes, and other geotechnical defects (Wu et al. 2004; Pei 2008; Shen et al. 2013; Zhang et al. 2014; Wang et al. 2017). In addition, coupled

hydro-mechanical problems are often observed in the laminated shale rock which causes strength degradation often leading to injuries related to roof fall incidents. Therefore, the pore pressure in joints is the key factor causing groundwater bursting and roof fall incidents (Wu et al. 2004; Zhang et al. 2014). It is significant to investigate the effect of pore pressure in joints on rock strength, which can offer the theoretical supports for solving the problem of groundwater bursting and roof failure with laminations.

On one hand, the research about the effect of joints on rock strength has been highlighted by different methods in the past. Kulatilake et al. (1997) investigated the jointed rock mass strength through physical modeling under uniaxial compressive loading, and found that orientation of joint sets played a significant role related to the models of failure. Cao et al. (2016) investigated the uniaxial compressive strength and failure patterns of ubiquitous-joint rock-like specimens by combining similar material testing and two-dimensional numerical simulation. Yang et al. (2017) studied the interaction of parallel joints and its effect on the mechanical behavior of jointed rock mass models. Alejano et al. (2017) performed triaxial strength tests on artificially jointed standard-size granite specimens with two sub-vertical and three sub-horizontal joints, and found that the Mohr–Coulomb and Hoek–Brown failure criteria were fit to peak and residual strength tests results. Wang et al. (2018) developed a modeling method to predict the failure behaviors of fiber-reinforced clay under the triaxial compression state. Huang et al. (2019) used UDEC rock mass two-dimensional models to research the effect of joint orientations on rock mass strength in an unconfined state. Li et al. (2021) conducted a series of uniaxial and triaxial compression tests on slate samples at different foliation orientations to investigate the size effect and anisotropy in slate. All the above research mainly focus on the pure mechanical effect of joints on the failure behavior of rock and obtained some valuable results.

On the other hand, besides the pure mechanical effect, many scholars studied the hydro-mechanical couplings between the solid phase of rock and the pore fluid, which is also playing an important role in rock deformation. Li et al. (2008) developed a shear-flow testing apparatus for rock fractures and carried out shear-flow coupling tests to evaluate the influence of morphological properties of rock fractures on their hydro-mechanical behavior (Li et al. 2008). Asahina et al. (2019) characterized the hydraulic and mechanical responses of Kimachi sandstone associated with fracture plane reactivation induced by elevated pore-fluid pressure (Asahina et al. 2019). Ke et al. (2020) explored the two-phase flow system inside the actual hydraulic geometry of a milling circuit hydrocyclone with the aid of both computational and experimental techniques (Ke et al. 2020). Neupane et al. (2020) measured the changes in pore pressure in the rock mass near the tunnel walls during load changes, and concluded that the development of hydraulic gradient and additional pore pressure acting on the rock blocks cause a delayed response from the rock mass during pressure transients (Neupane et al. 2020). Farahmand and Diederichs (2021) simulated the mechanical responses of the rock to analyze the role of interaction between the pore fluid and the rock (Farahmand and Diederichs 2021). The above studies provide useful insights to analyze the effect of the hydro-mechanical couplings on rock.

In summary, previous studies obtained meaningful results about the pure mechanical or coupled hydro-mechanical effect on the rock deformation from different perspectives. However, the effect of the joint pore pressure in parallel joints on the rock strength under the coupled hydro-mechanical state is not fully understood. In this paper, three-dimensional cylindrical models with different parallel oriented joints were designed. Uniaxial and triaxial compression tests were simulated under different joint pore pressures. Finally, the results compared with literatures and the couple effect of joint pore pressure and joint orientations on rock strength was discussed.

2 Modeling Strategy

3DEC (Distinct-Element Modeling of Jointed and Blocky Material in 3D) is a three-dimensional numerical modeling code for advanced geotechnical analysis of soil, rock, ground water, structural support, and masonry. One of its advantages is to offer a comprehensive set of capabilities for modeling fluid flow and the effect of fluid pressures on rock, thus, we choose it to investigate the couple effect of joint pore pressure and joint orientations on rock strength. In this paper, seven three-dimensional numerical models with parallel oriented joints at 0°, 15°, 30°, 45°, 60°, 75°, 90°

were developed by 3DEC. The numerical simulation schemes and models are shown in Fig. 1.

According to Fig. 1, the models are 50 mm in diameter and 100 mm in height. The joint spacing of each model is 5 mm. Two rigid plates at the bottom and top of each model were set 5 mm in height. The uniaxial and triaxial compression simulation tests were conducted to obtain the rock strength under uncoupled state and coupled hydro-mechanical state. The boundary conditions and the patterns of fluid flow through parallel joints are shown in Fig. 2.

The bottom plate was set to zero displacements along x-, y- and z- directions. The top plate was set to 10 mm/s of the axial strain-loading rate along z-directions for uniaxial and triaxial compression tests and zero displacements along x- and y- directions. When conducting the triaxial compression tests (Fig. 2b), the confining pressure were set at 10, 20, 30 and 40 MPa, respectively. When fluid involves, we set three directions of fluid flow through parallel joints (Fig. 2c–e) according to the different oriented joints. The pump was located at the left side of the model for horizontal joints and at top for vertical joints (Fig. 2c, d). Then, the fluid could pass through the all flow planes, and discharge from the right and bottom side of the rock specimens. However, when facing the inclined joints (15°, 30°, 45°, 60°, 75°), we set two pumps at the left and top side of the rock specimens simultaneously (Fig. 2e). In this case, some fluid would discharge from the right side and others from the bottom side.

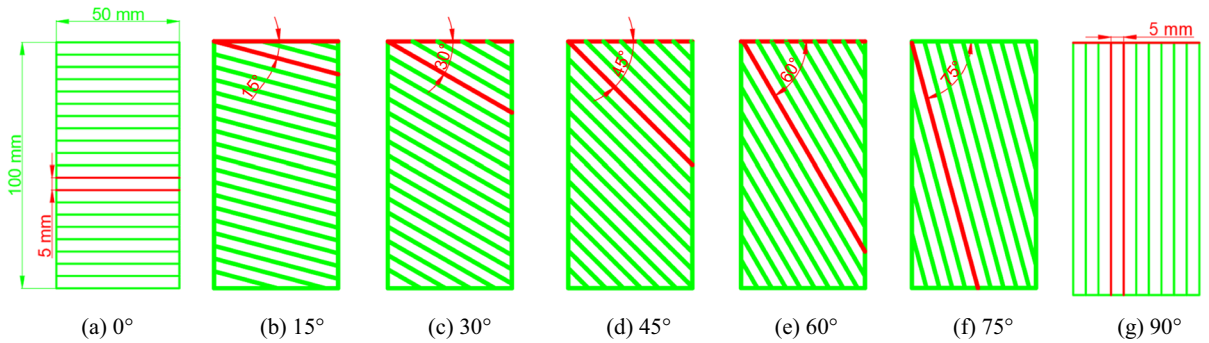

(a) 2D schemes with parallel oriented joints

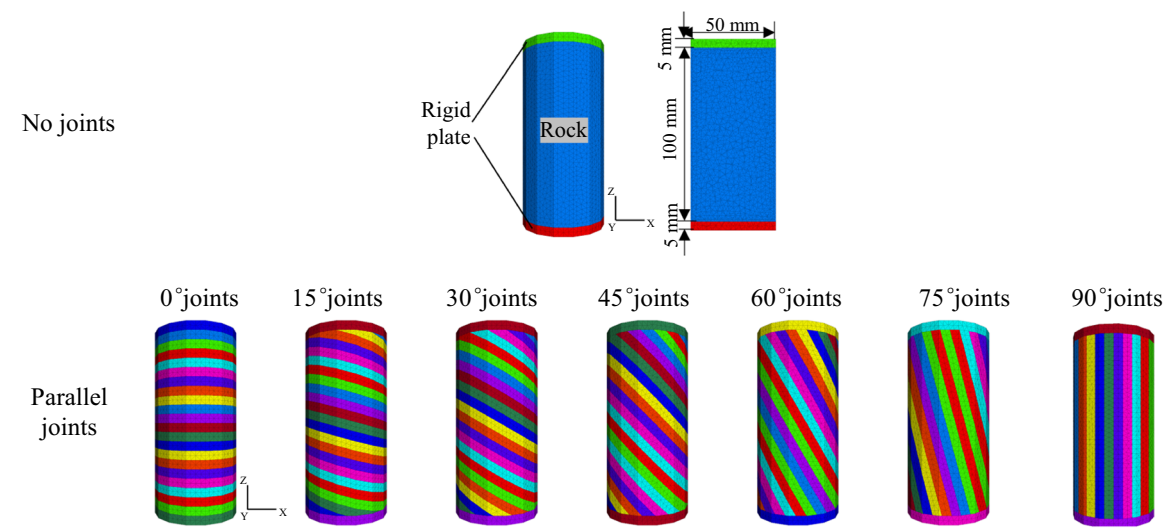

(b) 3D models generated by 3DEC

Fig. 1 Numerical simulation schemes and models

Fig. 2 Boundary conditions and directions of fluid flow through horizontal joints

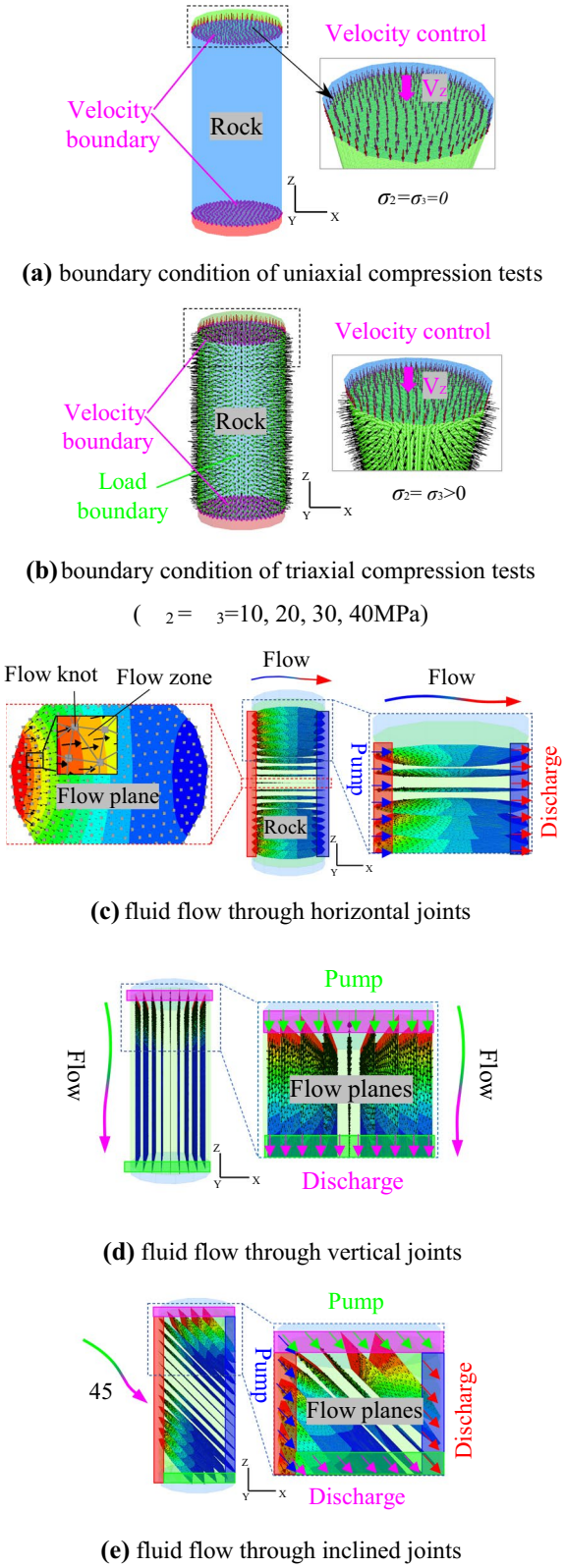

(a) boundary condition of uniaxial compression tests

(b) boundary condition of triaxial compression tests ($_2$ = $_3$=10, 20, 30, 40MPa)

(c) fluid flow through horizontal joints

(d) fluid flow through vertical joints

(e) fluid flow through inclined joints

There are three components involved in this research, i.e., rock (matrix), joint (contact) and fluid (pore pressure). The chosen constitutive model for rock is Mohr–Coulomb model, which is a conventional model used to represent shear failures in rocks. The model for joint is Mohr–Coulomb Joint model, which simulates displacement-weakening of the joint by loss of cohesive and tensile strength at the onset of shear or tensile failure. Fully coupled hydro-mechanical model was applied when fluid involves. In this case, rock deformation influence the fluid pressures, and the fluid pressures also affect the rock stresses and strains.

In addition, it is important to note that in laboratory test, the specimen in a triaxial state is jacketed and the confining pressure is applied by pressuring the fluid around the specimen. The only two places which are not jacketed are the top and the bottom end of the specimens which are in contact with the platens. The top platens have holes which introduces the fluid, and the discharge is collected through the lower platen. In this research, however, we set three flow patterns presented above, which ensure that fluid could pass through all flow planes. We have assumed that the rock and the platen are frictionless boundaries for obtaining more accurate rock strength. In actual tests, some initial confining pressure is first introduced and then the axial stress is applied to reach a hydrostatic state followed by introduction of the pore pressure. In this numerical modeling, we took into account the above specific procedures.

3 Calibration of Numerical Models

3.1 Calibration of Uncoupled Mechanical Modeling

According to the above-established models, the reliability of the input parameters for rock and joints would be tested in this section. The input parameters for the above models are shown in Table 1.

The uniaxial and triaxial compressive tests were conducted under the uncoupled state with the Mohr–Coulomb constitutive model for rock and joints. Stress–strain curves under 0, 10, 20, 30 and 40 MPa of confining pressures of different joint

Table 1 Input parameters of rock and joints

Density ρ (kg/m^3)	Elastic modulus E (GPa)	Poisson's ratio μ	Cohesion C (MPa)	Internal friction angle φ (°)	Tensile strength σ_T (MPa)
Rock material properties					
2500	55	0.15	18	39	8.00
Density ρ (kg/m^3)	Bulk modulus K_j (GPa)	Shear modulus G_j (GPa)	Cohesion C_j (MPa)	Internal friction angle φ_j (°)	Tensile strength σ_{Tj} (MPa)
Rock joints properties					
0	800	400	4	38	4.00

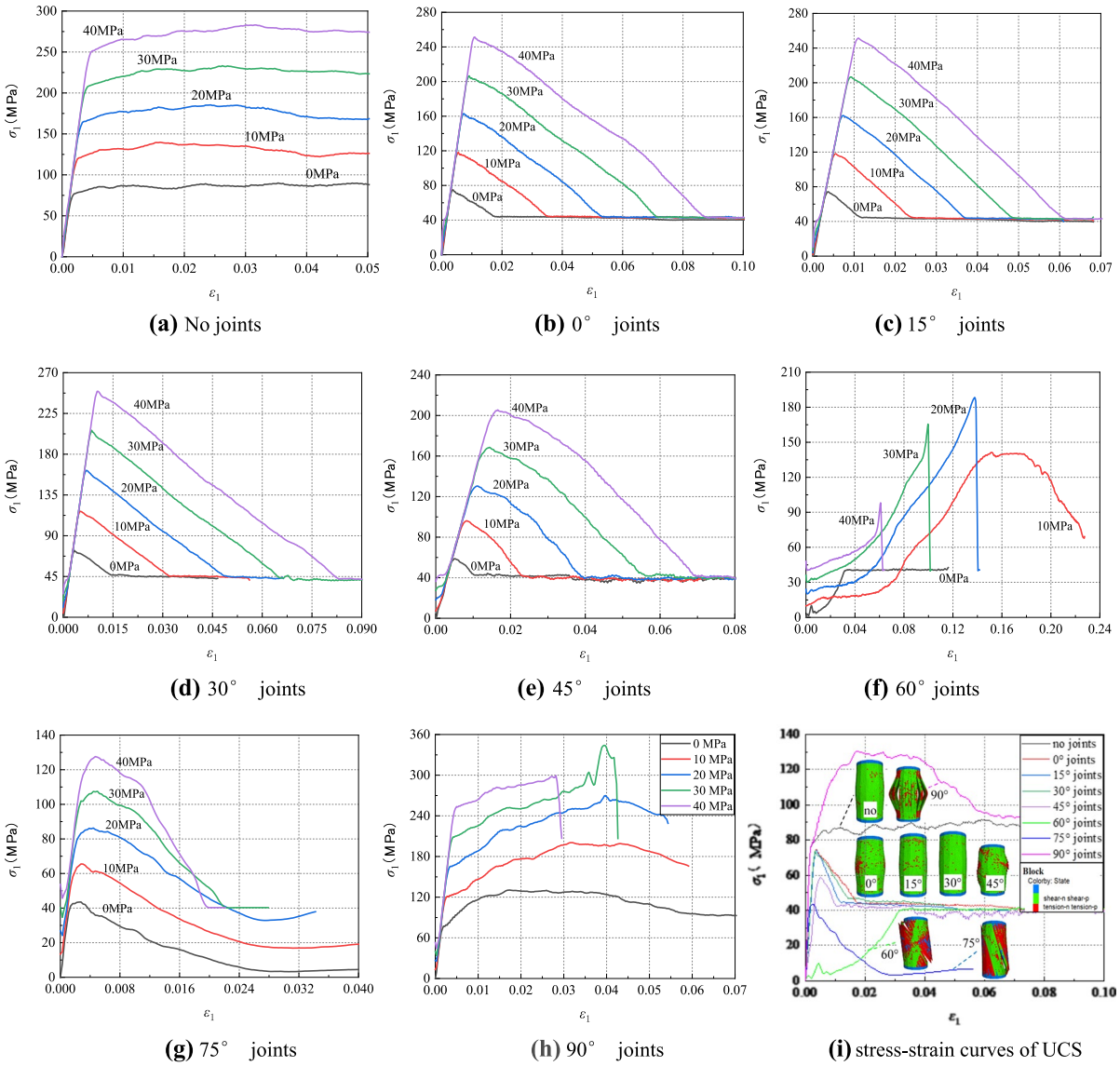

(a) No joints **(b)** 0° joints **(c)** 15° joints

(d) 30° joints **(e)** 45° joints **(f)** 60° joints

(g) 75° joints **(h)** 90° joints **(i)** stress-strain curves of UCS

Fig. 3 Stress–strain curves of different parallel oriented joints rock specimens models

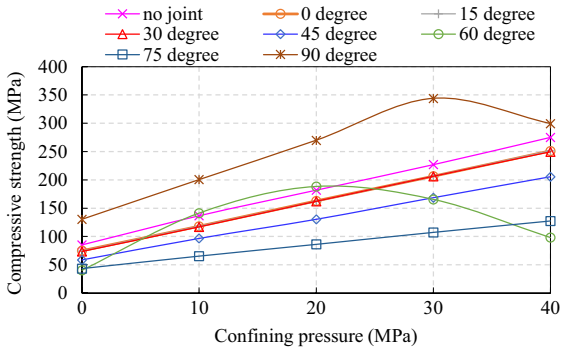

(a) Curves of rock strength versus confining pressure

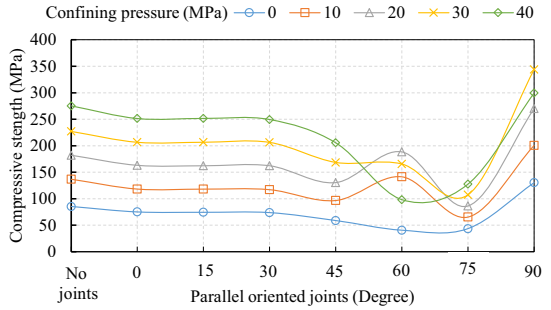

(b) Curves of rock strength versus parallel oriented joints

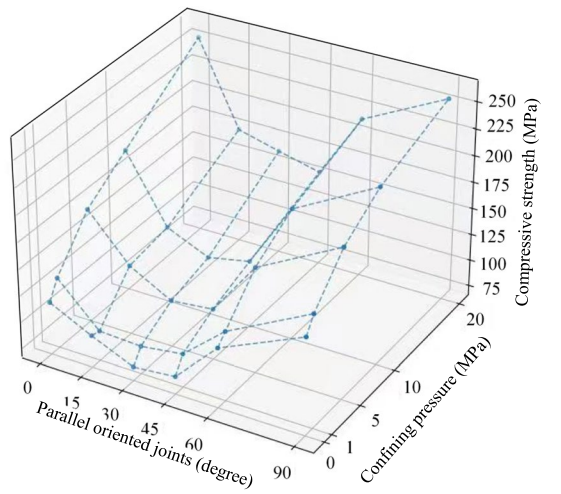

(c) the classic "U"-shaped curve (Li et al. 2021)

Fig. 4 Curves for describing influence of confining pressure and parallel oriented joints on compressive strength

orientations obtained from the 3DEC simulation are shown in Fig. 3a–h. Specially, Fig. 3i shows the stress–strain curves of UCS (Unconfined Compression Test) for different parallel oriented joints models.

Table 2 Numerical modeling input parameters of fluid properties

Density ρ_w (kg/m^3)	Bulk modulus K_w (GPa)	Viscosity η (Pa·s)	Aperture at zero stress azero (mm)	Residual aperture ares (mm)	Max-aperture amax (mm)
1000	2.00	0.001	0.10	0.01	1.00

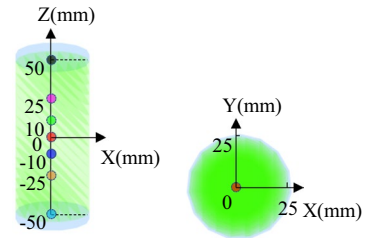

(a) observation fluid knotslocations

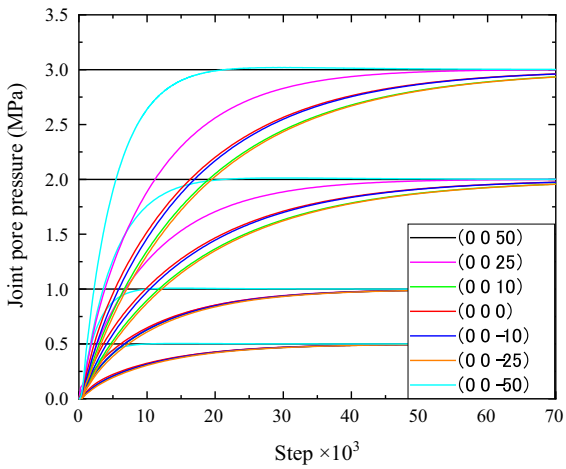

(b) balancedjoint pore pressure curves

Fig. 5 Testing method and results

In Fig. 3, σ_1 refers to axial stress, and ε_1 refers to axial strain. From the stress–strain curves, we can obtain rock strength (uniaxial compressive strength and triaxial compressive strength). In order to clearly reflect the effects of confining pressure and joint orientations, the curves of rock strength versus confining pressure and curves of rock strength versus parallel oriented joints are shown in Fig. 4a and b.

From Fig. 4a, at 0°, 15°, 30°, 45° and 75° orientations rock strength presents a linear growth with

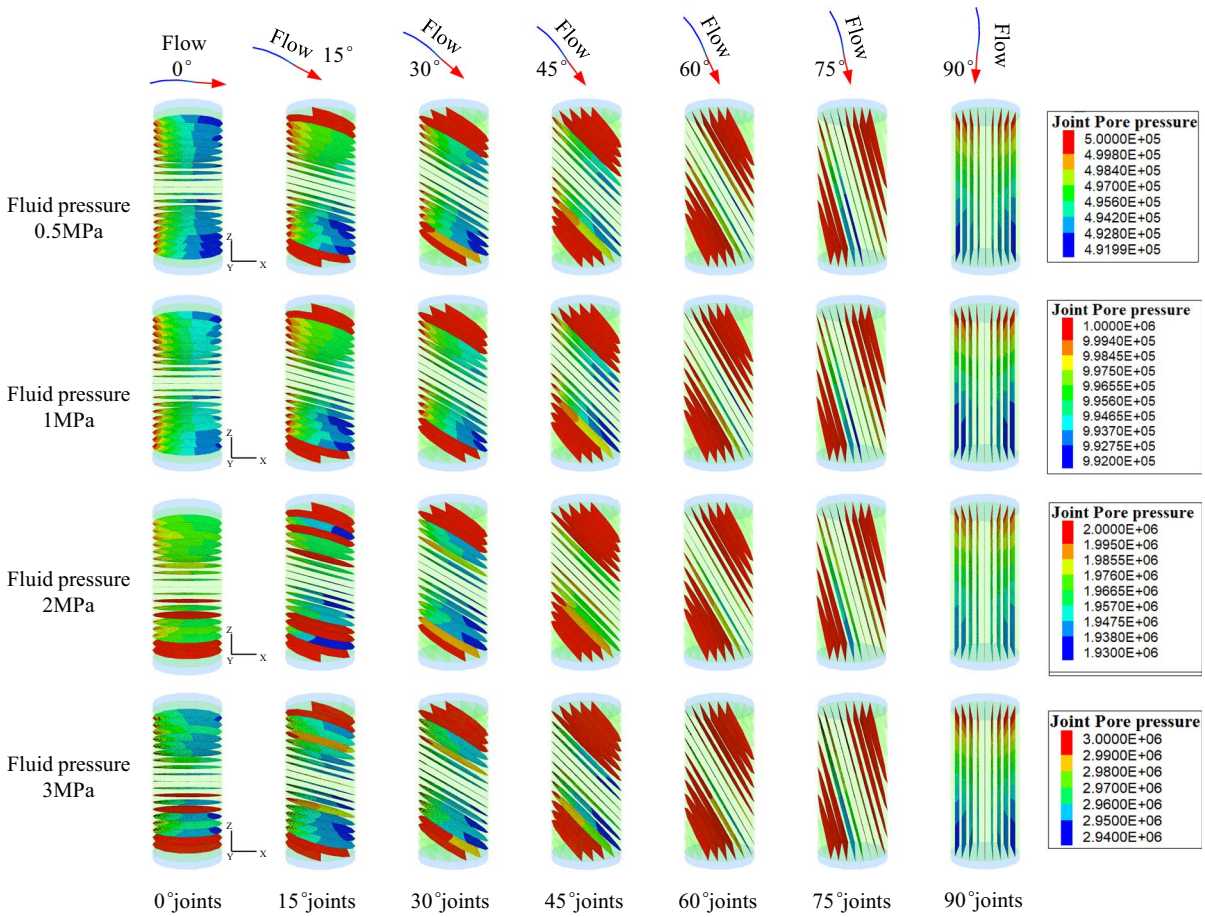

Fig. 6 Final balance state of joint pore pressure of each rock specimen model after fluid flow through parallel oriented joints

the increase of the confining pressure. However, in the both cases of 65° and 90° rock strength presents a growth until the confining pressure increases at 20 MPa and 30 MPa, respectively. Figure 4b shows that the rock strength decrease until the orientation reaches at 75°. Rock strength varies with different orientations producing the classic "U"-shaped curve, as shown in Fig. 4c (Yang et al. 2017; Li et al. 2021). Therefore, the above input parameters are valid.

3.2 Calibration of Coupled Hydro-Mechanical Modeling

In this paper, fully coupled hydromechanical simulation is conducted. The solution is performed by alternating frequently between mechanical and fluid calculations. During the simulation progress, the time associated with mechanical deformation is significantly less than that associated with fluid flow. The fluid material properties required for analysis are shown in Table 2. For testing the reliability of these parameters, the method and results are shown in Fig. 5.

Seven observation fluid knots were set at the center of each model for measuring the joint pore pressure (Fig. 5a). From Fig. 5b, the joint pore pressure presented the logarithmically growth with the stepwise increase. Finally, four joint pore pressure (0.5, 1.0, 2.0, 3.0 MPa) were achieved. The final balanced state of joint pore pressure is shown in Fig. 6. The right legend in Fig. 6 indicates that all flow planes inside each model reached the joint pore pressure we set. Therefore, the input parameters of fluid properties are reliable.

Table 3 Rock strength under the couple effect of joint pore pressure and joint orientations

Joint pore-pressure (MPa)	Confining pressure (MPa)	Joint orientations						
		0°	15°	30°	45°	60°	75°	90°
0.5	0	145.63	97.83	171.92	76.88	7.04	40.67	74.88
	10	253.37	161.37	272.59	109.50	12.68	66.07	120.52
	20	319.37	227.49	327.18	147.17	21.51	89.24	164.30
	30	384.17	292.18	381.97	185.38	31.15	112.93	208.71
	40	447.75	358.45	433.68	225.38	40.98	136.88	252.75
1.0	0	145.76	96.10	172.39	85.49	11.27	40.02	74.15
	10	253.69	162.50	274.11	165.25	12.27	64.94	120.74
	20	319.14	227.27	328.15	211.13	22.76	88.06	163.79
	30	383.64	290.98	381.07	245.42	31.48	111.62	209.04
	40	454.03	357.72	431.61	281.43	41.61	135.99	252.27
2.0	0	146.07	96.24	172.25	6.32	39.08	35.91	74.29
	10	253.44	162.33	270.88	13.71	13.34	62.07	119.80
	20	317.23	227.10	325.44	26.07	22.95	86.08	164.13
	30	389.06	290.50	376.66	38.66	31.72	110.14	208.76
	40	456.17	356.95	430.51	49.21	41.98	134.75	252.10
3.0	0	146.16	73.91	171.71	7.19	40.29	32.33	71.84
	10	253.03	117.76	270.03	16.66	16.93	57.86	118.01
	20	316.07	160.91	322.20	27.90	28.50	82.44	163.91
	30	375.91	204.95	369.95	38.80	38.53	107.14	206.08
	40	455.12	247.40	426.75	48.78	42.94	132.42	250.66

4 Results and Analysis

The tests were conducted with the joint pore pressure maintained constant (Rutqvist and Stephansson 2003), and the corresponding strain-strength curves were obtained for calculating rock strength. Due to the space limits, the strain-strength curves were not presented, but the final rock strength was listed under the couple effect of joint pore pressure and joint orientations in Table 3.

According to the results in Table 3, curves for describing rock strength under the couple effect of joint pore pressure and joint orientations are shown in Fig. 7.

From Fig. 7, the maximum strength is achieved at 0° orientation, while the minimum is at the 60° or 45°. A slight increase in the strength is presented at the 30° due to the couple effect of the pore pressure and the orientation of joints. The curve changed from the classic "U"-shaped curve (Fig. 4) to a "W"-shaped curve due to the joint pore pressure.

In order to further analyze the couple effect of joint pore pressure and joint orientations on rock strength, relationship between the rock strength and joint pore pressure with different confining pressure are shown in Fig. 8.

From Fig. 8, the strength presents a slight decrease with the increase of the joint pore pressure from 0.5 to 3 MPa at the orientations of at 0°, 30°, 75° and 90° (Fig. 8a, c, f, g). The strength at 15° (Fig. 8b) keeps a constant until the joint pore pressure reaches at 2 MPa and then decreases rapidly. The strength at 45° (Fig. 8d) increases firstly and then decreases. However, the strength at 60° (Fig. 8e) show a growth tendencies as the joint pore pressure increases. Therefore, an increase in the joint pore pressure has different effects on the rock strength due to different joint orientations.

5 Discussion

Typically, groundwater bursting is the problem of fluid flow in rock masses, which is a hydro-mechanically coupled problem. That is, pore pressures affect the mechanical deformation, and mechanical

Fig. 8 Relationship between rock strength and joint pore pressure with different confining pressure ▶

deformation affects pressures. Therefore, there are three aspects of hydro-mechanical coupling in a

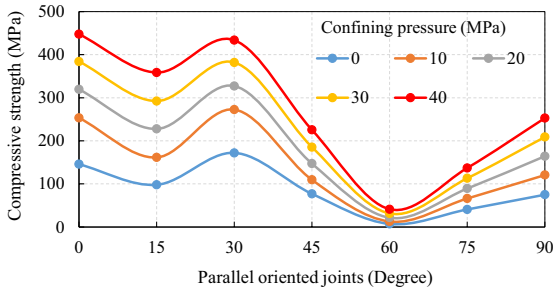

(a) Joint pore pressure 0.5 MPa

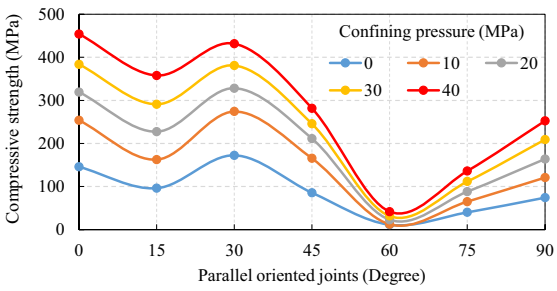

(b) Joint pore pressure 1 MPa

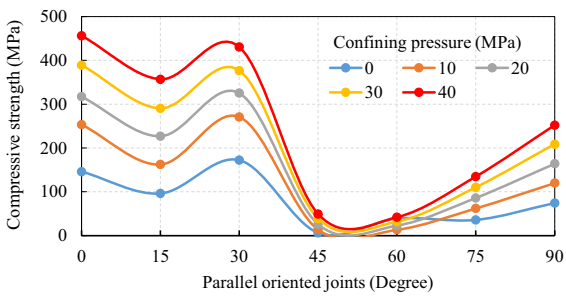

(c) Joint pore pressure 2 MPa

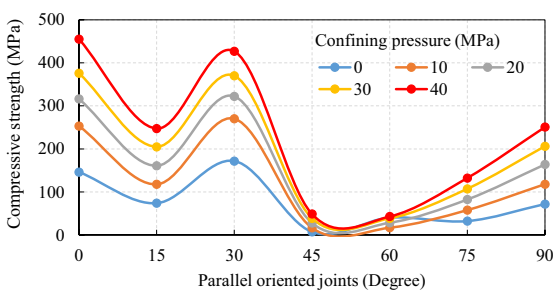

(d) Joint pore pressure is 3 Mpa

Fig. 7 Curves for describing rock strength under the couple effect of joint pore pressure and joint orientations

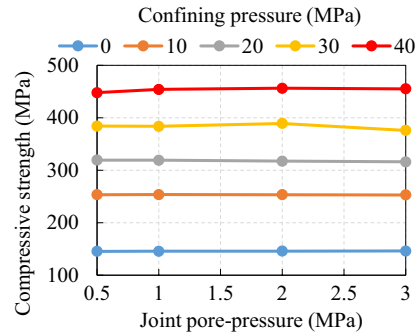

(a) 0° joints

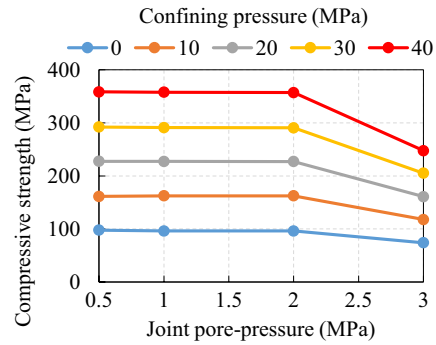

(b) 15° joints

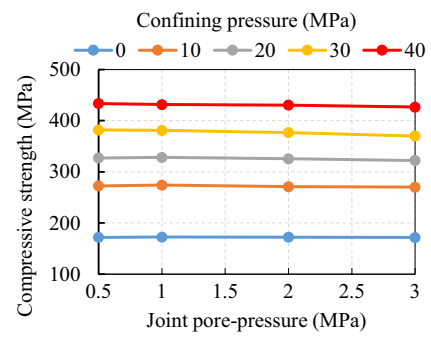

(c) 30° joints

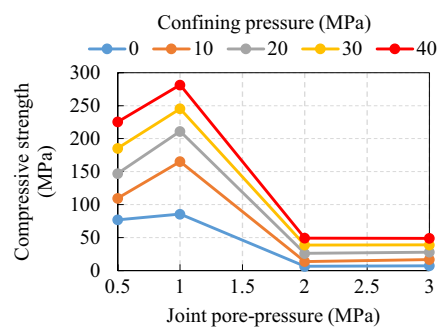

(d) 45° joints

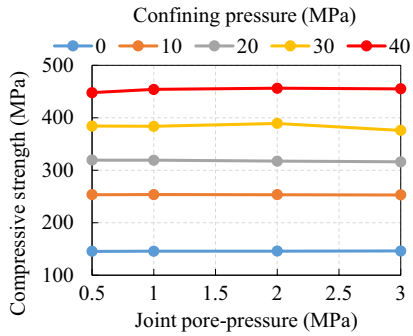

(a) 0° joints

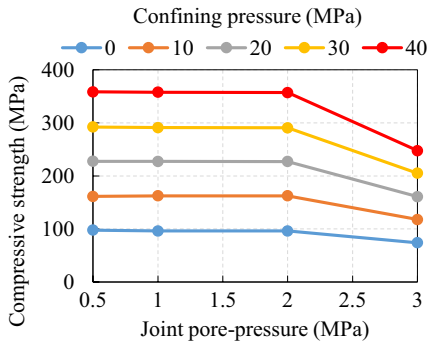

(b) 15° joints

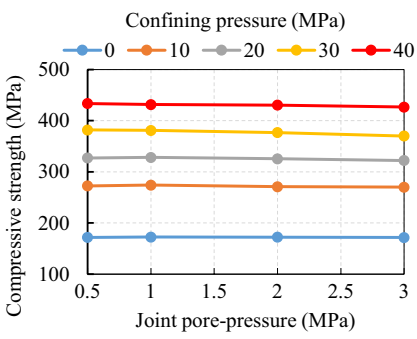

(c) 30° joints

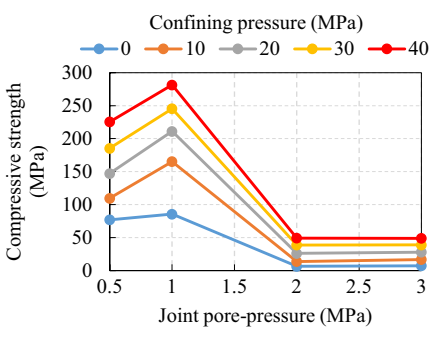

(d) 45° joints

Fig. 8 (continued)

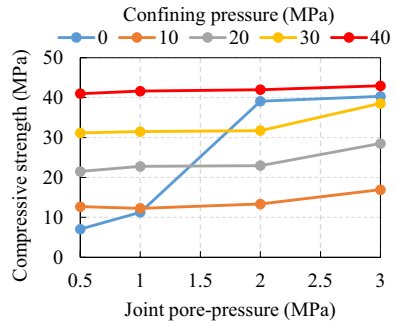

(e) 60° joints

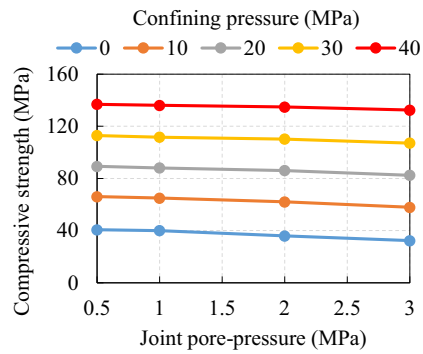

(f) 75° joints

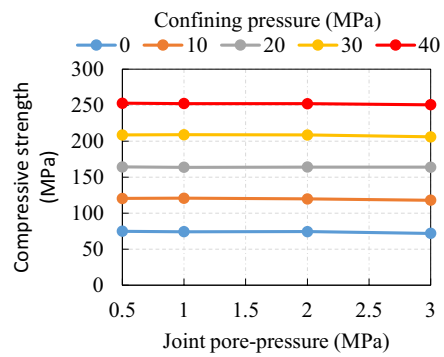

(g) 90° joints

Fig. 8 (continued)

fractured rock mass: (1) the effect of pore pressure on strength of fractured rock masses, (2) the effect of mechanical deformation on permeability, and (3) the effect of mechanical deformation on pore pressures. In this study, the effect of the joint pore pressure in parallel oriented joints on rock strength was investigated for attempting to reveal the above first aspects. The fractured rock masses were simplified by rock samples fractured with parallel oriented joints.

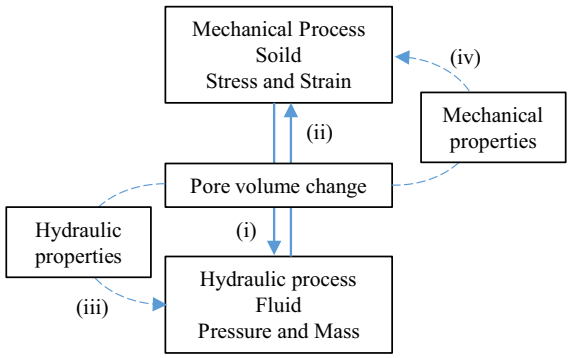

Fig. 9 Hydromechanical couplings in geogical media. (i) and (ii) are direct couplings through pore volume interactions, whereas (iii) and (iv) are indirect couplings through changes in material properties (Rutqvist and Stephansson 2003)

The classic "U"-shaped curve of rock strength with various orientations was obtained under uncoupled mechanical state. The curve changed to a "W"-shaped curve when the joint pore pressure was involved. Therefore, we found that besides the parallel oriented joints, the joint pore pressure has an extra effect on the deformation of the rock specimens. This extra effect by the joint pore pressure was mentioned by Rutqvist and Stephansson (2003) in Fig. 9, but it is not clear. In this paper, by numerical modeling we found that a slight increase in the strength is presented at the 30° orientations due to the combination effect of the pore pressure and the orientation of joints. The slight increase changes the classic "U"-shaped curve to "W"-shaped curve. It means that the extra effect occurs between 0° to 90° orientations, at 30° orientation in this numerical modeling, which needs to be further verified by laboratory tests in future work.

In addition, some scholars concluded that the effect of pore pressure on rock strength are negative without consider the factor of parallel oriented joints. For examples, Murrell (1965) found that an increase in the pore pressure has the same effect as a decrease in confining pressure on the strength based on the sandstone specimens (Fig. 10a) (Murrell 1965); Farahmand and Diederichs (2021) argued that the rock strength is negatively correlated with the pore pressure based on grain-based models (Fig. 10b) (Farahmand and Diederichs 2021). However, we found that the effect of pore pressure on rock strength depends on the joint orientations, and compared with pore pressure effects, the joint orientation has more effect on the compressive strength. For examples, the strengths at 0°, 15°, 30°, 75° and 90° orientations decrease with the increase of the joint pore pressure, while the strength at 60° increases as the joint pore pressure increases. It means that the increase of pore pressure probably leads the less effective stress, and at specific joint angle 60, the rock shows more strength. However, the strength at 45° increases firstly and then decreases. The results indicate that the joint orientation plays more important role than joint pore pressure on the strength change, thus needs to be considered for studying groundwater bursting.

It is important to note that few previous studies tested the effect of joint pore pressure on rock strength with different orientations. Therefore, the research results by numerical modeling in this paper

Fig. 10 Previous reference results about effect of pore pressure on rock failure modes and rock peak strength; σ_3 refers to confining pressure

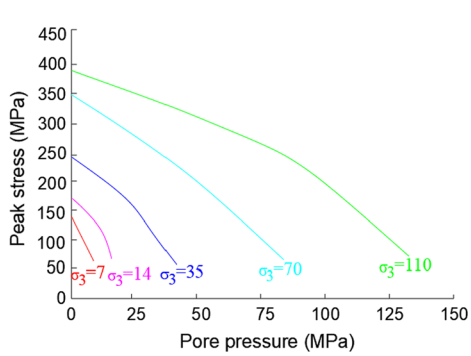

(a) Test results of Darley Dale sandstone with 21% porosity (Murrell 1965)

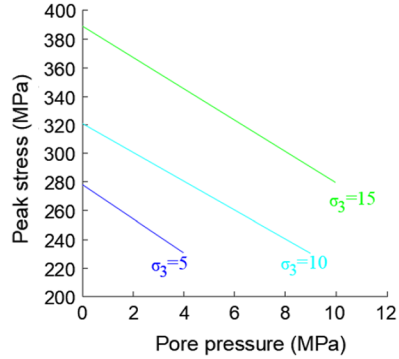

(b) Test results based on the grain-based model (Farahmand and Diederichs 2021)

needs to be further verified by laboratory tests in the future work.

6 Conclusions

1. Three-dimensional models with parallel oriented joints were developed by 3DEC. Uniaxial and triaxial compression tests were conducted under uncoupled mechanical state and coupled hydro-mechanical state with different joint pore pressure. The input parameters of rock, joints and fluid properties were calibrated based on the results of previous research.
2. The results show that the classic "U"-shaped curve of the rock strength with various joint orientations was obtained under the uncoupled mechanical state. The curve changed to "W"-shaped due to the effect of joint pore pressure.
3. Effect of joint pore pressure on rock strength depends on the joint orientations. The strength at 0°, 15°, 30°, 75° and 90° orientations decreases as the joint pore pressure increases; at 60° the strength increases; at 45° the strength increases firstly and then decreases.

Acknowledgements This investigation was financially supported by the Key Project of Natural Science Foundation of China (U21A20108) and the Project of Central Plans Science and Technology Innovation Leading Talents (224200510012). All authors would like to thank the organizations for supporting this investigation.

Data Availability Enquiries about data availability should be directed to the authors.

Declarations

Conflict of interest The authors have not disclosed any competing interests.

References

Alejano LR, Arzúa J, Bozorgzadeh N, Harrison JP (2017) Triaxial strength and deformability of intact and increasingly jointed granite samples. Int J Rock Mech Min Sci 95:87–103. https://doi.org/10.1016/j.ijrmms.2017.03.009

Asahina D, Pan PZ, Sato M et al (2019) Hydraulic and mechanical responses of porous sandstone during pore pressure-induced reactivation of fracture planes: an experimental study. Rock Mech Rock Eng 52:1645–1656. https://doi.org/10.1007/s00603-018-1706-8

Hong CR, Cao P, Fan X et al (2016) An experimental and numerical study on mechanical behavior of ubiquitous-joint brittle rock-like specimens under uniaxial compression. Rock Mech Rock Eng 49:4319–4338. https://doi.org/10.1007/s00603-016-1029-6

Esterhuizen GS, Klemetti T, Sears MM et al (2021) Assessing longwall gateroad ground response and support alternatives. Mining, Metall Explor 38:1739–1759. https://doi.org/10.1007/s42461-021-00430-x

Farahmand K, Diederichs MS (2021) Calibration of coupled hydro-mechanical properties of grain-based model for simulating fracture process and associated pore pressure evolution in excavation damage zone around deep tunnels. J Rock Mech Geotech Eng 13:60–83. https://doi.org/10.1016/j.jrmge.2020.06.006

Guo W, Zhao G, Bai E et al (2021) Effect of overburden bending deformation and alluvium mechanical parameters on surface subsidence due to longwall mining. Bull Eng Geol Environ 80:2751–2764. https://doi.org/10.1007/s10064-020-02091-4

Guo W, Zhao G, Lou G, Wang S (2019) A new method of predicting the height of the fractured water-conducting zone due to high-intensity longwall coal mining in China. Rock Mech Rock Eng 52:2789–2802. https://doi.org/10.1007/s00603-018-1567-1

Huang F, Shen J, Cai M, Xu C (2019) An empirical UCS model for anisotropic blocky rock masses. Rock Mech Rock Eng 52:3119–3131. https://doi.org/10.1007/s00603-019-01771-2

Ke R, Shingote C, Kadambi JR et al (2020) Experimental and numerical investigations of the fluid flow in a hydrocyclone with an air core. Mining, Metall Explor 37:277–286. https://doi.org/10.1007/s42461-019-00131-6

Kulatilake PHSW, He W, Um J, Wang H (1997) A physical model study of jointed rock mass strength under uniaxial compressive loading. Int J Rock Mech Min Sci Geomech Abstr 34:692–693. https://doi.org/10.1016/S1365-1609(97)00123-8

Li B, Jiang Y, Koyama T et al (2008) Experimental study of the hydro-mechanical behavior of rock joints using a parallel-plate model containing contact areas and artificial fractures. Int J Rock Mech Min Sci 45:362–375. https://doi.org/10.1016/j.ijrmms.2007.06.004

Li K, Yin ZY, Han D et al (2021) Size effect and anisotropy in a transversely isotropic rock under compressive conditions. Rock Mech Rock Eng 54:4639–4662. https://doi.org/10.1007/s00603-021-02558-0

Murrell SAF (1965) The effect of triaxial stress systems on the strength of rocks at atmospheric temperatures. Geophys J R Astron Soc 10:231–281. https://doi.org/10.1111/j.1365-246X.1965.tb03155.x

Neupane B, Panthi KK, Vereide K (2020) Effect of power plant operation on pore pressure in jointed rock mass of an unlined hydropower tunnel: an experimental study. Rock Mech Rock Eng 53:3073–3092. https://doi.org/10.1007/s00603-020-02090-7

Pei J (2008) Strength of transversely isotropic rocks. MS, Civ Environ Eng Massachusetts Inst Technol p 340

Peng SS, Cheng J, Du F, Xue Y (2019) Underground ground control monitoring and interpretation, and numerical modeling, and shield capacity design. Int J Min Sci Technol 29:79–85. https://doi.org/10.1016/j.ijmst.2018.11.026

Rutqvist J, Stephansson O (2003) The role of hydrochemical coupling in fractured rock engineering. Hydrogeol J 11:7–40. https://doi.org/10.1007/s10040-002-0241-5

Shen J, Karakus M, Xu C (2013) Chart-based slope stability assessment using the Generalized Hoek-Brown criterion. Int J Rock Mech Min Sci 64:210–219. https://doi.org/10.1016/j.ijrmms.2013.09.002

Wang Y, Guo P, Dai F et al (2018) Behavior and modeling of fiber-reinforced clay under triaxial compression by combining the superposition method with the energy-based homogenization technique. Int J Geomech 18:04018172. https://doi.org/10.1061/(asce)gm.1943-5622.0001313

Wang Y, Jing H, Su H, Xie J (2017) Effect of a fault fracture zone on the stability of tunnel-surrounding rock. Int J Geomech 17:04016135. https://doi.org/10.1061/(asce)gm.1943-5622.0000837

Wu Q, Wang M, Wu X (2004) Investigations of groundwater bursting into coal mine seam floors from fault zones. Int J Rock Mech Min Sci 41:557–571. https://doi.org/10.1016/j.ijrmms.2003.01.004

Yang XX, Jing HW, Tang CA, Yang SQ (2017) Effect of parallel joint interaction on mechanical behavior of jointed rock mass models. Int J Rock Mech Min Sci 92:40–53. https://doi.org/10.1016/j.ijrmms.2016.12.010

Zhang R, Jiang Z, Zhou H et al (2014) Groundwater outbursts from faults above a confined aquifer in the coal mining. Nat Hazards 71:1861–1872. https://doi.org/10.1007/s11069-013-0981-7

Zhao G, Guo W, Li X (2020) Mechanical properties of mega-thick alluvium and their influence on the surface subsidence. Geotech Geol Eng 38:137–149. https://doi.org/10.1007/s10706-019-01003-y

Terms and Conditions

Springer Nature journal content, brought to you courtesy of Springer Nature Customer Service Center GmbH (“Springer Nature”).
Springer Nature supports a reasonable amount of sharing of research papers by authors, subscribers and authorised users (“Users”), for small-scale personal, non-commercial use provided that all copyright, trade and service marks and other proprietary notices are maintained. By accessing, sharing, receiving or otherwise using the Springer Nature journal content you agree to these terms of use (“Terms”). For these purposes, Springer Nature considers academic use (by researchers and students) to be non-commercial.
These Terms are supplementary and will apply in addition to any applicable website terms and conditions, a relevant site licence or a personal subscription. These Terms will prevail over any conflict or ambiguity with regards to the relevant terms, a site licence or a personal subscription (to the extent of the conflict or ambiguity only). For Creative Commons-licensed articles, the terms of the Creative Commons license used will apply.
We collect and use personal data to provide access to the Springer Nature journal content. We may also use these personal data internally within ResearchGate and Springer Nature and as agreed share it, in an anonymised way, for purposes of tracking, analysis and reporting. We will not otherwise disclose your personal data outside the ResearchGate or the Springer Nature group of companies unless we have your permission as detailed in the Privacy Policy.
While Users may use the Springer Nature journal content for small scale, personal non-commercial use, it is important to note that Users may not:

1. use such content for the purpose of providing other users with access on a regular or large scale basis or as a means to circumvent access control;
2. use such content where to do so would be considered a criminal or statutory offence in any jurisdiction, or gives rise to civil liability, or is otherwise unlawful;
3. falsely or misleadingly imply or suggest endorsement, approval , sponsorship, or association unless explicitly agreed to by Springer Nature in writing;
4. use bots or other automated methods to access the content or redirect messages
5. override any security feature or exclusionary protocol; or
6. share the content in order to create substitute for Springer Nature products or services or a systematic database of Springer Nature journal content.

In line with the restriction against commercial use, Springer Nature does not permit the creation of a product or service that creates revenue, royalties, rent or income from our content or its inclusion as part of a paid for service or for other commercial gain. Springer Nature journal content cannot be used for inter-library loans and librarians may not upload Springer Nature journal content on a large scale into their, or any other, institutional repository.
These terms of use are reviewed regularly and may be amended at any time. Springer Nature is not obligated to publish any information or content on this website and may remove it or features or functionality at our sole discretion, at any time with or without notice. Springer Nature may revoke this licence to you at any time and remove access to any copies of the Springer Nature journal content which have been saved.
To the fullest extent permitted by law, Springer Nature makes no warranties, representations or guarantees to Users, either express or implied with respect to the Springer nature journal content and all parties disclaim and waive any implied warranties or warranties imposed by law, including merchantability or fitness for any particular purpose.
Please note that these rights do not automatically extend to content, data or other material published by Springer Nature that may be licensed from third parties.
If you would like to use or distribute our Springer Nature journal content to a wider audience or on a regular basis or in any other manner not expressly permitted by these Terms, please contact Springer Nature at

onlineservice@springernature.com